Visual Abstract

Structural health evaluation of arch bridge by field test and optimized BPNN algorithm

Jiachen She, Zhihua Xiong*, Zhuoxi Liang, Xulin Mou
College of Water Resources and Architectural Engineering, Northwest A&F University, Yangling, Shaanxi 712100, China
jiachen_she@nwafu.edu.cn
zh.xiong@nwsuaf.edu.cn, https://orcid.org/0000-0001-8796-1004
zx.liang@nwafu.edu.cn, 2022050878@nwafu.edu.cn

Yu Zhang
College of Civil Engineering and Architecture, Zhejiang University, Hangzhou, Zhejiang 310058, China
12212129@zju.edu.cn

ABSTRACT. Arch bridges play an important role in rural roads in China. Due to insufficient funds and a lack of management techniques, many rural arch bridges are in a state of disrepair, unable to meet the increasing transportation needs. Thus, it is of great significance to develop a set of rapid and economic damage identification procedures for the management and maintenance of old arch bridges. Sanliushui Bridge, located in Chenggu County, Hanzhong, is selected as a model case. Field tests and numerical simulations were carried out to identify the damage states of Sanliushui Bridge. Wavelet Packet Energy change Rate Sum Square (WPERSS), a damage identification index based on wavelet packet analysis method was implemented to process the measured data of the load test and the simulated data of the numerical calculation model with assumed damage. Back Propagation Neural Network (BPNN), Genetic Algorithm-based BPNN (GA-BPNN), Particle Swarm Optimization Algorithm-based BPNN (PSO-BPNN) approaches and test data analysis are adopted to compare the measured data with the simulated data to quantitatively identify the damage degree of the selected bridge. By comparing the results of the two methods mentioned above, it is found that the proposed damage identification approach realized a precise damage identification of the selected arch bridges.

KEYWORDS. Arch bridge, Wavelet packet, Damage identification, Back propagation neural network, Test, Particle swarm optimization.

OPEN ACCESS

Citation: She, J. C., Xiong, Z. H., Liang, Z. X., Mou, X. L., Zhang, Y., Structural Health Evaluation of Arch Bridge by Field Test and Optimized BPNN Algorithm, Frattura ed Integrità Strutturale, 65 (2023) 160-177.

Received: 21.02.2023
Accepted: 27.05.2023
Online first: 31.05.2023
Published: 01.07.2023

INTRODUCTION

Facing the performance degradation of a massive number of old arch bridges in rural regions and the improving transportation demand in China, it is urgently required to develop a rapid system to identify the damage of these old arch bridges. Local governments are unable to adopt the expensive Structural Health Monitoring (SHM) equipment because of the lack of funds for maintenance management.

At present, the typical SHM mainly includes: systems based on static data and dynamic data. The large stiffness of arch bridge structures usually results in small deflection under the traffic load. The dynamic monitoring approach overcomes the disadvantage of the ones based on static tests that have high accuracy requirements, most of them obtain parameters such as frequency and mode by Fourier transform or wavelet transform [1-2]. However, Fourier transform is difficult to effectively analyze the high-frequency modes with the form of most structural damage signals and wavelet transform ignores the high-frequency part of the signal, which is not suitable for processing signals with medium and high-frequency information as the main components [3]. Alternatively, the wavelet packet analysis method, featuring its ability to decompose both the low-frequency part and high-frequency part of the signal, can become an efficient method to decompose the signal containing medium and high-frequency information [4-5]. According to the wavelet packet decomposition, Zhu Jinsong et al. [6] proposed a damage identification index- Wavelet Packet Energy change Rate Sum Square (WPERSS) and they carried out a damage identification of a bridge based on this index. Yue Pan et al. took the operation stage of Wangzong Tunnel of Wuhan Metro Line 3 as an example to conduct structural health monitoring and evaluation by analyzing acceleration response signals with wavelet packet energy theory, and effectively realized real-time identification of structural damage and early structural damage alarm [7].

Recently, SHM based on machine learning (ML) has become the dominant approach, which is supported by multi-source data and is capable of effectively realizing accurate separation of monitoring data under the influence of a complex environment [8].

ML algorithms provide necessary tools to enhance the function of SHM system. Hence the comprehensive application of ML algorithms and SHM methods have attracted much attention [9], Moisés Silva et al. carried out genetic algorithm (GA) to achieve an efficient and accurate damage detection for bridge structures [10], and Osama Abdeljaber et al. successfully estimated the actual damage amount of nine damage situations by using one-dimensional Convolutional Neural Network (CNN) [11]. Nevertheless, on account of a single ML algorithm usually has various defects. For example, back propagation neural network (BPNN) has strong nonlinear mapping ability, self-learning ability, and adaptability, but it is easy to get stuck in the local minimum situation, and its convergence rate is slow [12], artificial neural network (ANN) has high classification accuracy in various application fields, but it is also easy to fall into the local minimum trap [13], support vector machine (SVM) has been widely used in SHM field because of its effectiveness in classification, training, construction and regression tasks, but it has a disadvantage of long computation time and lack of interpretability of results [14]. Using optimization algorithms to make up for the defects of a single ML algorithm and to achieve efficient and accurate structural health monitoring has become a research hotspot. Guoqing Gui et al. showed that the three optimized SVM methods can realize the accurate health monitoring of civil engineering structures, and their sensitivity, accuracy, and effectiveness are significantly better than traditional SVM methods [15], Giuseppe Santarsiero et al. proposed an artificial neural network (ANN) optimized by particle swarm optimization (PSO) which can monitor the performance of reinforced concrete structures effectively [16].

Although many effective methods have been proposed in the field of bridge structural damage identification, most of these methods need to rely on professional equipment or laboratories, the cost of which is unaffordable for less-developed regions. Therefore, this paper aims to build a set of low-cost bridge damage identification methods which can meet the requirements of engineering evaluation, so as to make independent identification of bridge damage feasible in less-developed rural areas. In this study, the wavelet packet analysis method of SHM methods based on dynamic index and the intelligent computation method that uses optimization algorithms together with ML algorithms method of SHM methods based on intelligent computation are combined on the basis of existing research results. And an old bridge is selected to verify the damage identification systems proposed by the author. The results of this study may provide alternative insights for bridge damage identification and benefit economic development in less-developed regions.

METHODOLOGY

Assuming that the acceleration signal of bridge is f, wavelet packet analysis can decompose f to the i^{th} scale and obtain 2^i nodes. If j is set as the number of the nodes of ith scale, then $f_{i,j}$ is the structural response signal on the ith scale node (i, j), and E_i, j, the energy of $f_{i,j}$, is shown as Eqn. (1) [17]:

$$E_{i,j} = \sum \left| f_{i,j} \right|^2 (j = 0,1,..,2^i\text{-}1) \tag{1}$$

The characteristics of the bridge structure can be reflected by the wavelet packet energy spectrum vector of the structural response signal at the node (E_i):

$$E_i = \{E_{i,j}\}(j = 0,1,..,2^i - 1) \tag{2}$$

The terminal frequency of the structural response signal will also fluctuate when the bridge structure is damaged, which will lead to the change of the energy of some nodes decomposed by wavelet packet. The damage to the bridge structure can be judged because the energy of each node is very sensitive to the fluctuation of the response signal. In order to identify the damage to the bridge structure effectively, WPERSS based on the wavelet packet analysis method is chosen as the damage identification index, which is shown as Eqn. (3):

$$WPERSS = \sum_{j=0}^{2^i-1} \left[\frac{(E_{f_i^j})_b - (E_{f_i^j})_a}{(E_{f_i^j})_a} \right]^2 = \sum_{i=1}^{m} \left[\frac{(E_{f_i^j})_b}{(E_{f_i^j})_a} - 1 \right]^2 \tag{3}$$

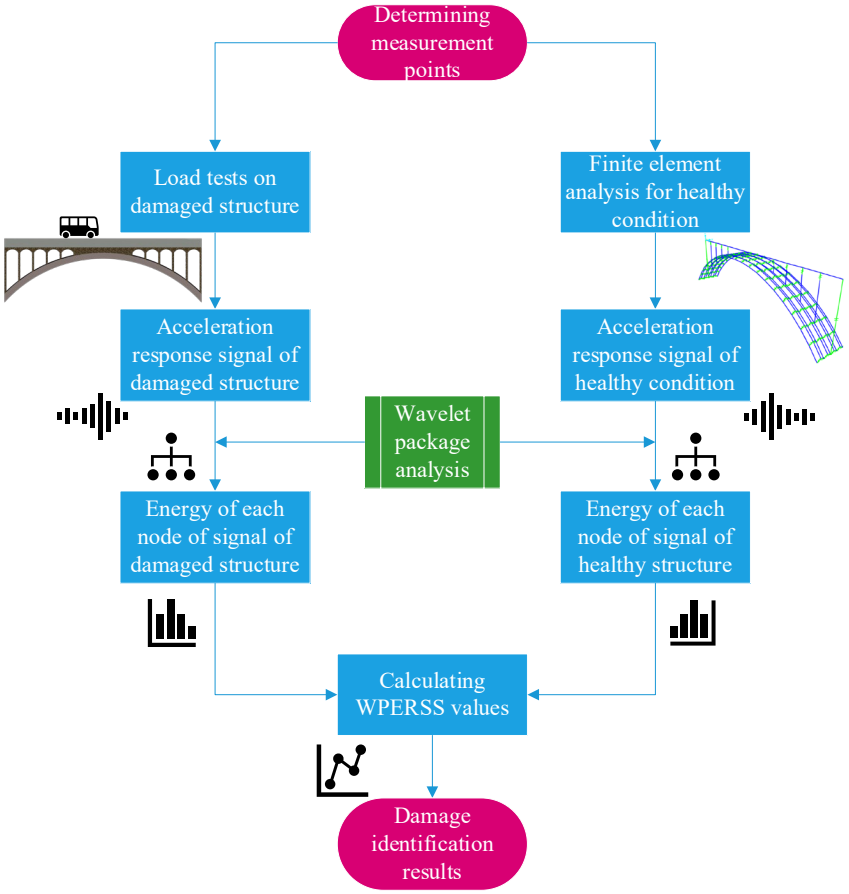

Figure 1: The flow chart of damage identification.

In Eqn. (3), the energy of the healthy bridge structure response signal is $(E_{fj})_b$, the energy of a damaged bridge structure response signal is $(E_{fj})_a$, the scale, or the number of decomposition layers is i, and the total number of wavelet packet decomposition frequency bands is $m=2^i-1$.

The application of the damage identification index is illustrated in Fig. 1. Firstly, the acceleration response signal of the healthy bridge structure and the damaged bridge structure are decomposed by wavelet packet to obtain several nodes respectively, and then the energy of each node is calculated as Eqn. (1). After finding the energy of all nodes of the healthy bridge structure and the damaged bridge structure, the WPERSS value is obtained by combining the corresponding node energy of the healthy bridge structure and the damaged bridge structure as Eqn. (3). The acceleration response signal of the healthy bridge structure is derived from the finite element model, and the acceleration response signal of the damaged bridge structure is determined from the finite element model with assumed damage or collected by the accelerometers in the load test. Finally, test data analysis and machine learning methods are carried out to compare WPERSS values of the simulated damage and WPERSS values of the load test to derive the damage identification results.

INTRODUCTION OF THE TESTED BRIDGE

Sanliushui bridge, a typical old arch bridge with a total length of 73.7 m and a width of 8.0 m, which was built in 1977 and opened to traffic in 1982, is located in Shuidou Village of Chenggu County. Although remote from cities, this arch bridge in Fig.2 is a vital lifeline structure for the local transport. The bridge is comprised of a superstructure of double curved arch and substructure of gravity abutment. The main arch rib has a depth of 1.2 m, while the depth of other ribs is 0.89 m. The axis of the arch is catenary, with a clear height of 12.6 m at the top of the arch. The bridge deck's thickness is 0.3 m. The damage to the bridge is serious due to long-term service, which makes the scientific maintenance of the bridge extremely urgent. According to the bridge inspection report provided by the local bureau of transport, there were many cracks in the arches and arch ribs of the bridge. Some concrete spalling, exposed bars and local voids in arches were observed. Therefore, it is of great practical significance to carry out load tests and damage identification on Sanliushui bridge.

Figure 2: Sanliushui bridge.

FIELD TEST

After communicating with the local bureau of transport, a representative vehicle of the local was selected as the test vehicle and the speed of the test vehicle was determined according to the operating speed of the local vehicles. A vehicle weighted 33.6 kN is displayed in Fig.3, with a front axle weight of 15.60 kN and a rear axle weight of 18.20 kN, was used to simulate the live load excitation at the speed of 30 km/h, 40 km/h, and 50 km/h, respectively. Meanwhile, portable acceleration sensors which are all set on the bridge deck with a sampling frequency of 10 Hz were used to collect acceleration time history signals of each point under the live load of the vehicle at different speeds. These points are on the bridge deck and will be specified later.

Figure 3: Test vehicle.

The measurement locations for the collection of acceleration response signals were analyzed before the test. When selecting the measurement points, the numerical analysis model of the tested bridge was developed by CSI Bridge. In the finite element (FE) model, the bridge is subject to a vehicle load whose both axes weigh 7500 N and whose wheelbase is 1.5 m on the model at the speed of 10 m/s, 15 m/s, and 20 m/s, respectively, to gain the acceleration response signal of each joint in the model. The vehicle load was determined in accordance with the General Specifications for Design of Highway Bridges and Culverts (JTG D60-2015) [18]. The unit of vehicle speed was determined as "m/s" in order to match the settings in CSI Bridge, while the speed followed the road speed limits of Chinese Traffic Regulations. The FE model of the bridge was consisted of frame elements, and the arch ribs and deck are connected by the fully constrained connection element, which is shown in Fig. 4.

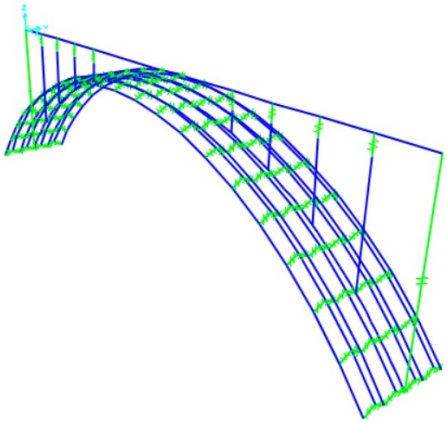

Figure 4: The FE model of Sanliushui bridge.

In terms of material properties, C50 concrete is used for bridge decks, arch ribs, and web arches, and stones are used for spandrel arches. Specific material properties are shown in Tab. 1.

Materials	Elasticity Modulus	Poisson's Ratio	Weight (Density)	Coefficient of Linear Expansion
Stone	5.5×10^4	0.168	25	1.17×10^{-5}
C50 concrete	3.45×10^4	0.2	25	1×10^{-5}
Stone	5.5×10^4	0.168	25	1.17×10^{-5}
C50 concrete	3.45×10^4	0.2	25	1×10^{-5}

Table 1: Material properties of FE components.

The acceleration response signals of 19 joints were selected in the FE model, including the foot of each spandrel arch, the mid-point of the arch, the mid-point of the main arch to the left, and joint to the right of the midpoint of the main arch. The initial damage status of the bridge was set through stiffness reduction.

The damage identification index, WPERSS was used to process the acceleration data under different vehicle speeds. The WPERSS value curves under different vehicle speeds are plotted in Fig. 5, in which the mutations of WPERSS curve at point 3(the midpoint of the second spandrel arch), point 4(the midpoint of the third spandrel arch), point 13(the right arch foot of the second spandrel arch), point 14(the midpoint of the main arch) and point 18(joint to the right of the midpoint of the main arch) are the most significant, and the relevant studies have shown that these points are more prone to damage [7]. Therefore, these points are selected as the acceleration measurement points.

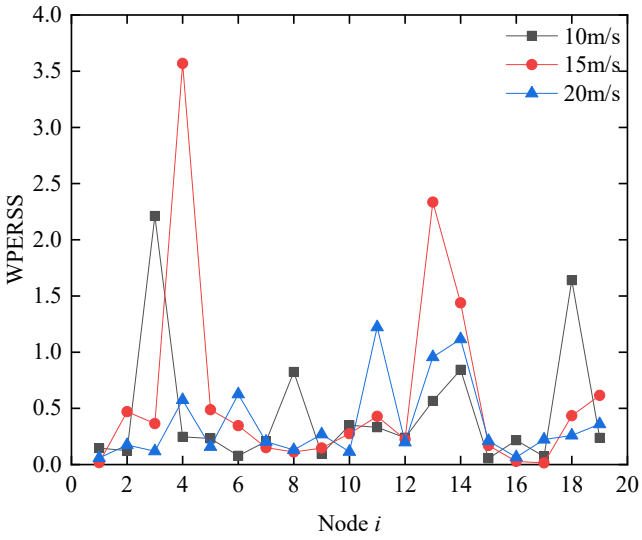

Figure 5: WPERSS value of each joint under different speed conditions.

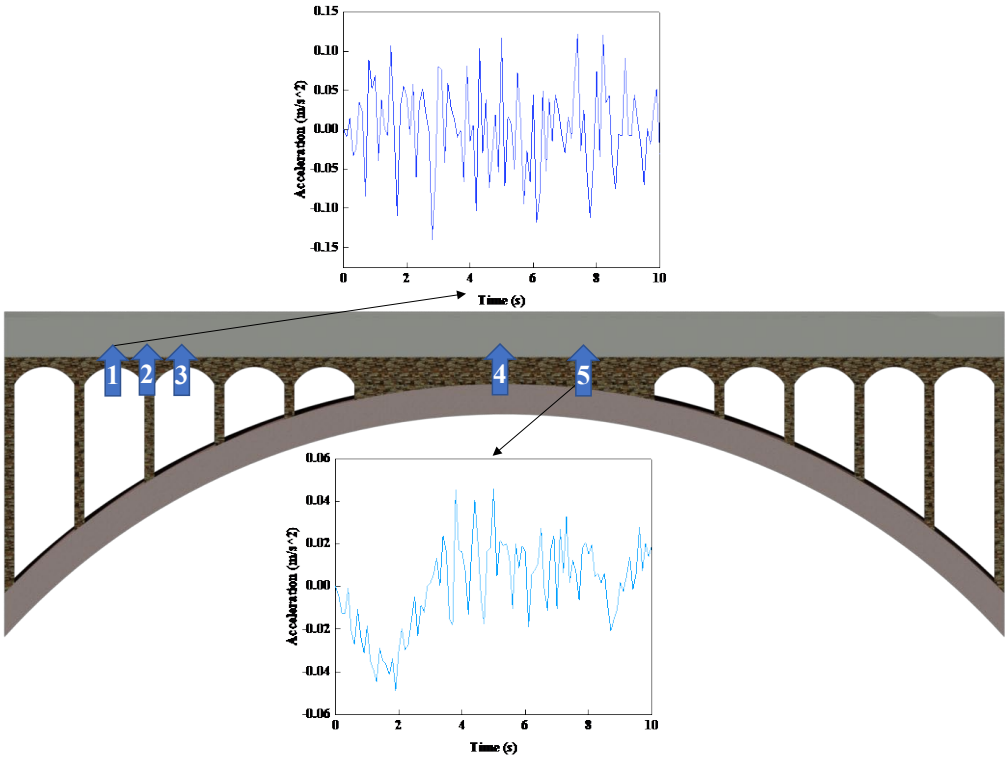

Figure 6: Schematic diagram of the layout of load test measuring point.

According to the result of the pre-test analysis, a total of 5 points in Fig. 6 are selected, which from left to right are the middle point of the second spandrel arch (point 1), the right arch foot of the second spandrel arch (point 2), the middle point of the third spandrel arch (point 3), the crown of the main arch (point 4), and the joint to the right of the midpoint of the arch (point 5). After the load test, Matlab has been applied to draw the acceleration-time curve of acceleration response signals, and the field test scenario is shown in Fig. 7.

a) Pre-test preparation.

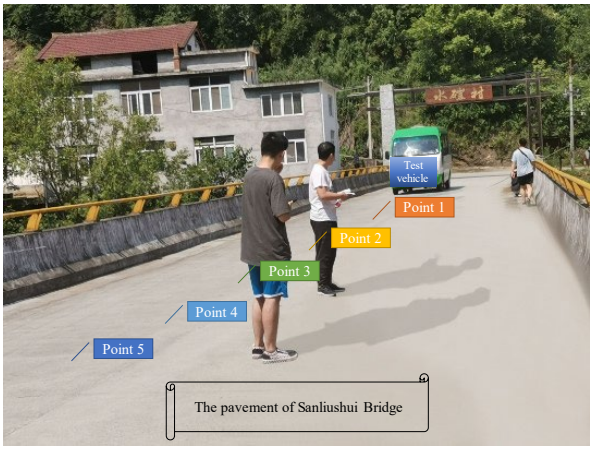

b) Ongoing test

Figure 7: Field test.

BRIDGE DAMAGE IDENTIFICATION

A vehicle same as the test vehicle in Fig.3 was input as an environmental excitation in the numeric analysis for damage identification. In addition, the arrangement of acceleration measurement points is the same as the arrangement of load test measurement points in Fig. 6. The sampling frequency of the acceleration response signal is 10 Hz, and the sampling time is 10 s.

DB20 wavelet was chosen to decompose the acceleration time history signal to the third or fourth scale based on the field test [19]. The stiffness of elements near the points is reduced by multiplying the stiffness by a factor, such as 0.9, in the FE model to simulate the damage of measurement points. As a matter of comprehensively and objectively explaining the damage identification effect through the WPERSS value, the WPERSS value will be normalized as Eqn. (4):

$$R_{ij} = \frac{WPERSS_{ij}}{\max WPERSS_{ij}} \tag{4}$$

For illustrating the performance of the WPERSS in damage localization, the working conditions with the vehicle traveling at 30km/h and different damage degrees at single or several measurement points, and DB20 wavelets are selected to decompose the acceleration signal to the third scale (i=3). WPERSS values are calculated as Eqn. (3) and the WPERSS values under different working conditions at the same measurement point are normalized as Eqn. (4), which are shown in Fig. 8. The damage location in Fig. 8(a) is point 1, while the damage location in Fig. 8(b) is point 4 and 5. Clearly, the WPERSS values of the damage position vary greatly with the damage degree, especially the difference between the WPERSS value of 20% damage and that of 30% damage, the former is about 20% of the latter, but in the healthy position, the former is about 50% of the latter. Therefore, WPERSS is capable to identify single and multiple damaged locations.

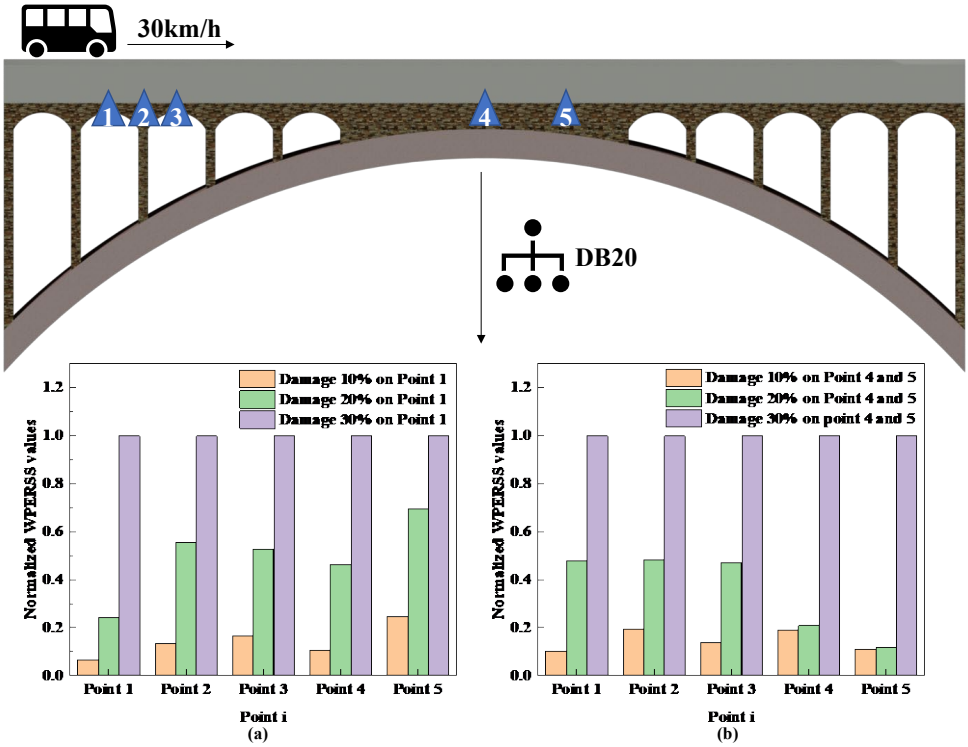

Figure 8: Normalized WPERSS values with different damage degrees at single or several measurement points. Normalized WPERSS values with different damage degrees on Point 1. Normalized WPERSS values with different damage degrees on Point 4 and 5.

In order to illustrate the influence of the damage degree of measurement points on the damage identification effect, the working conditions with the vehicle traveling at 40 km/h and different degrees of damage at each point and DB20 wavelet to decompose the acceleration signal into the third (i=3) and fourth scales (i=4) were chosen for comparison, which are shown in Fig. 9(a) and Fig. 9(b). WPERSS values were calculated and normalized as Eqn. (3) and Eqn. (4), which are shown in Fig. 9. By comparison, it can be seen that the WPERSS value is positively correlated with the damage degree of the point, and the above relationship is still effective when the scale of wavelet packet decomposition is different, and the WPERSS value does not change significantly with the variation of vehicle speed as well observed from Fig. 10(a), which contribute to estimating the damage degree of bridge structure by the WPERSS value.

The average value of the WPERSS value at the same speed was normalized as Eqn. (4), which is shown in Fig. 10. By comparison, it can be seen that when the scale of wavelet packet decomposition is different, the WPERSS value does not change significantly with the change of vehicle speed, which indicates that the WPERSS value has no obvious relationship with vehicle speed, and the vehicle speed and the scale of wavelet packet decomposition do not affect the damage identification effect.

The working conditions with different degrees of damage at each point with the vehicle running at the speed of 50 km/h were selected and ordinary noise was added to the acceleration time signal based on the Sound Environment Quality Standard of China [20] to illustrate the influence of noise on the damage identification effect. The changes of the acceleration signal before and after adding noise are shown in Fig. 11. The acceleration time-history signal in Fig. 11 is obtained in the FE model with a truck speed of 30 km/h and 20% damage on point 3. DB20 wavelet was selected to decompose the acceleration time signal with 70 dB noise into the third (i=3) and fourth (i=4) scales as plotted in Fig. 12(a) and Fig. 12(b).

WPERSS value was calculated and normalized as shown in Fig. 12. By comparison, it can be found that the WPERSS value is positively correlated with the damage degree of the measurement points under different degrees of noise and different scales of wavelet packet decomposition, which proves that it is still feasible to judge the damage degree of the bridge structure by the WPERSS value in the influence of noise, and ordinary noise does not affect the damage identification effect.

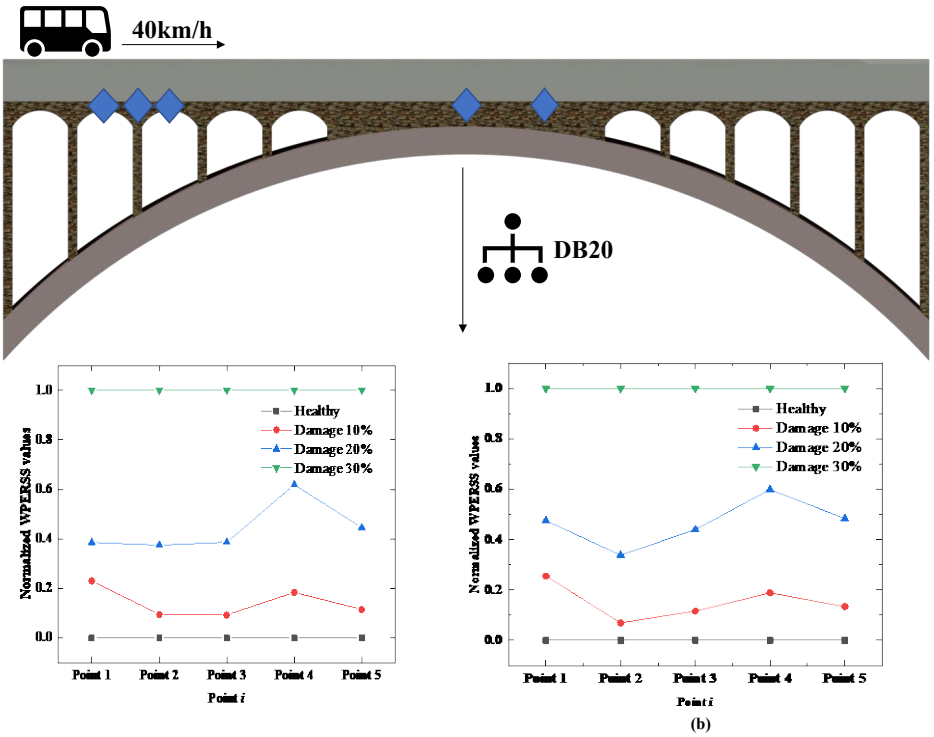

Figure 9: Normalized WPERSS values with different damage degrees and wavelet packet decomposition degrees. Normalized WPERSS values with different damage degrees when wavelet packet decomposition degree is third scale (i=3). Normalized WPERSS values with different damage degrees when wavelet packet decomposition degree is fourth scale (i=4).

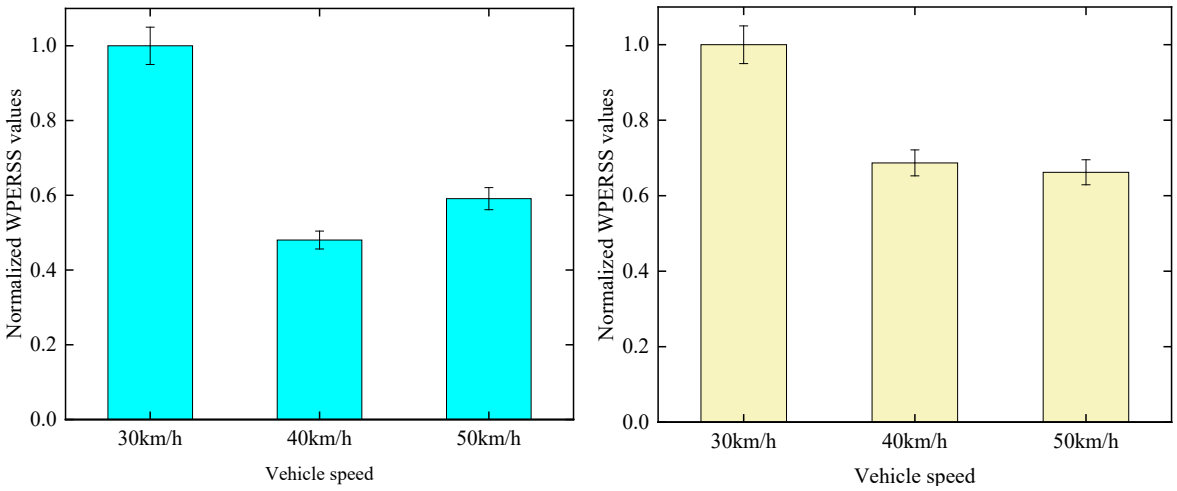

Figure 10: Normalized average value of WPERSS values with different wavelet packet decomposition degrees and vehicle speed. b) Normalized average value of WPERSS values with different vehicle speed when wavelet packet decomposition degree is third scale (i=3). b)Normalized average value of WPERSS values with different vehicle speeds when wavelet packet decomposition degree is fourth scale (i=4).

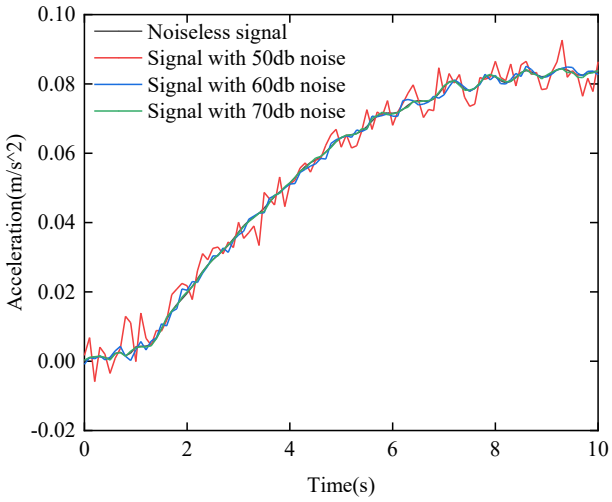

Figure 11: Comparison of acceleration time curve and without noise and with added noise.

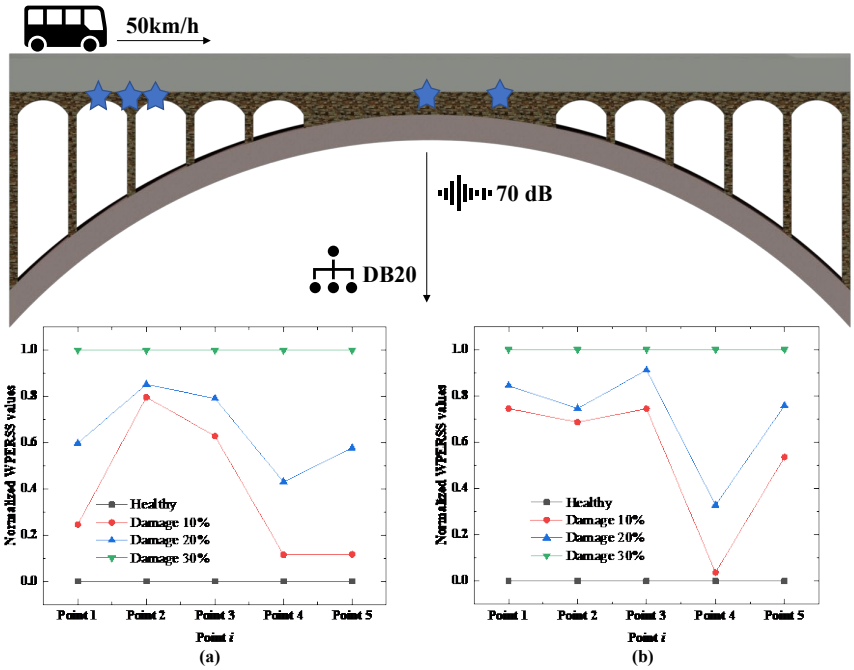

Figure 12: Normalized WPERSS values with the speed of 50km/h after adding 70dB noise. a) Normalized WPERSS values with the speed of 50km/h after adding 70dB noise when wavelet packet decomposition degree is third scale (i=3). b)Normalized WPERSS values with the speed of 50km/h after adding 70dB noise when wavelet packet decomposition degree is fourth scale (i=4).

WPERSS is not generally affected by the scale of wavelet packet decomposition, vehicle speed or ordinary noise. It does well in bridge damage identification, and the WPERSS value is positively correlated with the damage degree.
DB20 wavelet was selected to decompose the acceleration time signals of the load test to the second scale, and the signal simulated by CSI Bridge was also decomposed to the second scale to calculate the WPERSS value (Fig. 13). The comparison of the WPERSS value between the simulated and measured data at each measuring point when the driving speed was 30 km/h is shown in Fig. 13(a). While the comparison of WPERSS values between simulated and measured data at each measuring point when the driving speed is 40 km/h is shown in Fig. 13(b), and the comparison of WPERSS values between simulated and measured data at each measuring point when the driving speed is 50 km/h is shown in Fig. 13(c). Obviously, Fig. 13 further confirms that there is a positive correlation between the WPERSS values and the damage degree, i.e., the

higher the damage degree at the same location is, the larger the WPERSS value. We can determine the damage degree of each measurement point with the application of this relationship in Fig. 13.
According to Fig. 13, the damage degree of point 1, point 2, and point 3 are similar and serious, about 30%. The damage degree of point 4 and point 5 are mild, about 25%. The damage of point 5 is between point 1, or point 2, and point 3, or point 4, which is about 30%.

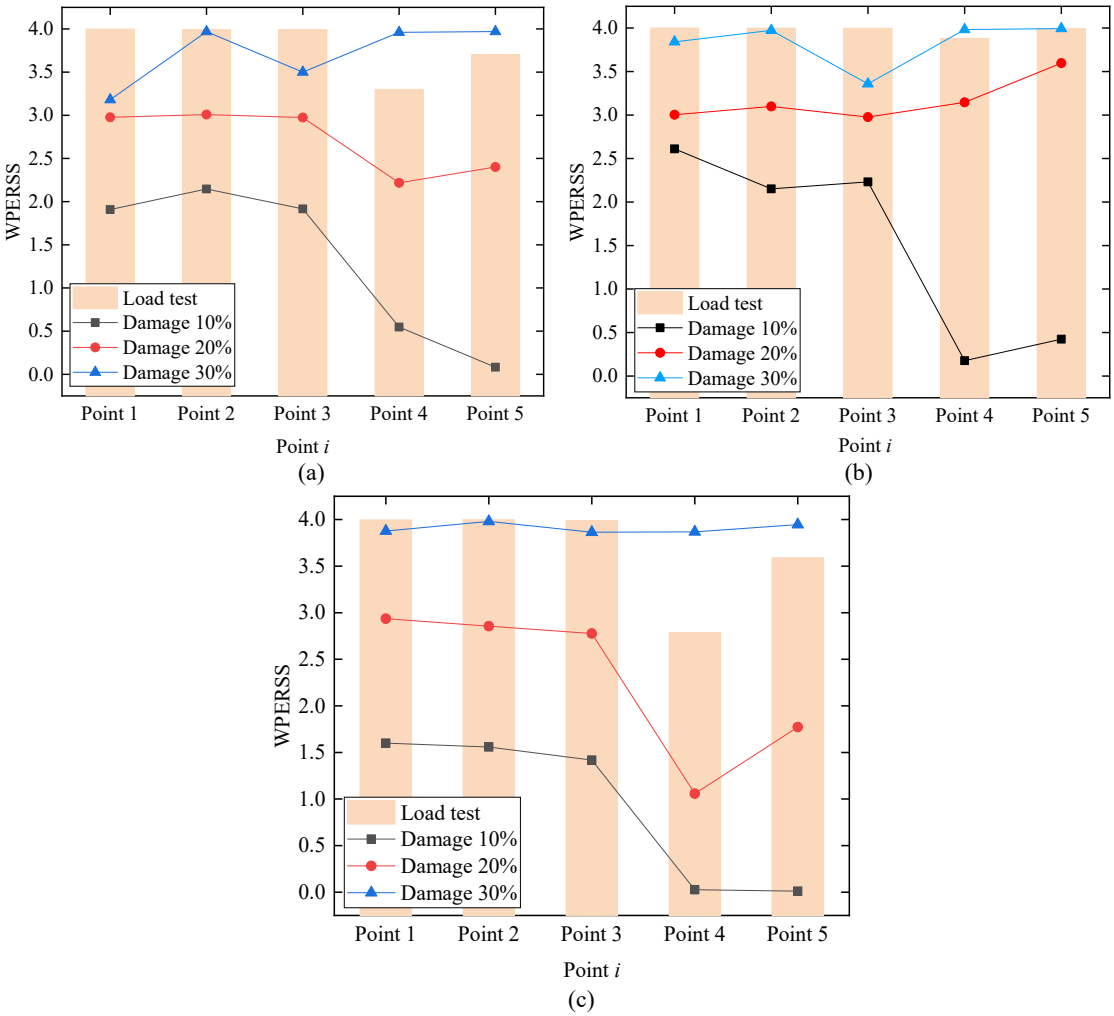

Figure 13: WPERSS value of each measuring point under speed conditions of 30km/h(a), 40km/h(b) and 50km/h(c).

DAMAGE IDENTIFICATION MODEL BASED ON BPNN

Back Propagation Neural Network (BPNN) is a feed forward neural network with at least three layers [21]. The three layers are input layer, hidden layer, and output layer. It has been widely used not only for identification but also for classification and prediction [22-26]. Compared with BPNN, predictions of Random Forest Algorithm (RF) tend to be biased towards less extreme values in some situations. Nevertheless, the RF models are complex and are not easy to interpret [27, 28].
However, one of the disadvantages of BPNN is that improper selection of initial weights and thresholds of the model may lead to local convergence and a slow convergence rate. This defect can be remedied by optimizing the initial value of BPNN model with an optimization algorithm. Four popular algorithms are compared to decide optimization algorithm for BPNN mode and summarized in Tab. 2: Particle Swarm Optimization Algorithm (PSO), Whale Optimization Algorithm (WOA), Moth Flame Optimization Algorithm (MFO), and Genetic Algorithm (GA) [29-32].

GA and PSO were both used in this paper to optimize the initial value of BPNN model. BPNN, GA-based BPNN optimization method (GA-BPNN), and PSO-based BPNN optimization method (PSO-BPNN) were used to identify the damage to the bridge. Their results were compared with the results of the load test analysis in Fig. 13 mentioned above. Three-layer BPNN is selected to develop the damage identification model, whose structure is shown in Fig. 14.

Methods	Advantages/Disadvantages
Moth Flame Optimization Algorithm (MFO)	Fall into local optimum easily; Unsatisfactory convergence speed.
Whale Optimization Algorithm (WOA)	Slow convergence speed; Tend to fall into local optimum in update mechanism.
Genetic Algorithm (GA)	Parallel, efficient and global; . Ability to find the global optimal solution adaptively.
Particle Swarm Optimization Algorithm (PSO)	Simple, easy to understand, and stable; Low dependence on empirical parameters.

Table 2: Comparison of optimization algorithms.

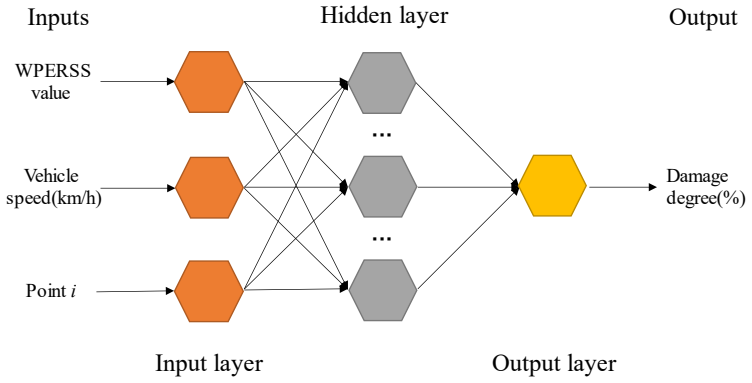

(a) Three-layer BPNN Structure

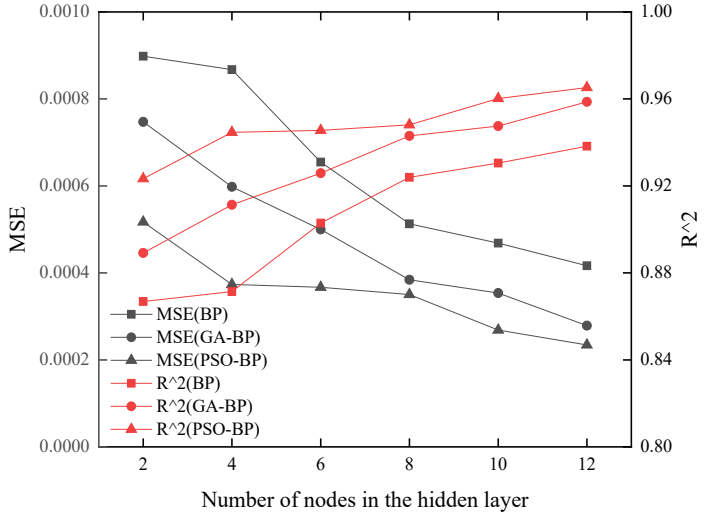

(b) Training Effects of BPNN, GA-BPNN and PSO-BPNN

Fig.14: Structure diagram of 3-layer BP neural network model.

The number of input layers is set as 1, and there are 3 input nodes, corresponding to 3 indicators that affect the damage degree: WPERSS value, vehicle speed, and different points. The number of output layers is 1, and there is 1 node in total, corresponding to the damage degree. The training data is 70% of the total data and the test data is 30% of the total data.

The number of hidden layers is also 1, and the number of nodes in the hidden layers, n, directly affects the convergence speed and accuracy of the model, which can generally be determined by Eqn. (5), (6) and (7) [33]:

$$n = \sqrt{x+1} + a \tag{5}$$

$$n = \sqrt{xy} \tag{6}$$

$$n = \log_2 x \tag{7}$$

In Eqn. (5), (6), and (7), the number of nodes in the hidden layer is n, the number of nodes in the input layer is x, the number of nodes in the output layer is y, and a is a constant ranging from 1 to 10. According to Eqn. (5), it can be concluded that the number of nodes in the hidden layer of this model ranges from 3 to 12. According to Eqn. (6) and (7), the number of nodes in the hidden layer approaches 2. In order to explore the most appropriate number of hidden layer nodes, n=2, 4, 6, 8, 10, and 12 were respectively chosen to build multiple BPNN models and compared. The model with the smallest error and the best fitting effect was taken as the damage identification model of Sanliushui bridge. The training effect of neural network models is shown in Fig. 14. It can be seen that with the increase of the number of hidden layer nodes n, the mean square error (MSE) decreases continuously, while the coefficient of determination (R2) increases continuously and approaches 1.

It is obvious that when the number of hidden layer nodes is set as 12, the MSE is the smallest, which means the error between predicted and actual values is the smallest; while the R2 is the highest, which means the effect of the fitting is the best. Therefore, the model is selected as the damage identification model of the bridge based on BPNN.

Optimizing the damage identification model using GA And PSO

The general procedure of the GA optimization is as follows:

1) Build a BPNN model and randomly select the initial weights and thresholds.
2) Using GA to find the best initial weights and thresholds of the BPNN model.
3) Assign the optimal initial weights and thresholds to the BPNN model to complete the optimization and make predictions.

The initial parameters of the GA are defined as: the number of evolutionary generations and iterations are both 20, the population size is 10, the crossover probability is 0.2, and the variation probability is 0.1. The structure and relevant parameters of the BPNN used in the optimization algorithm are the same as those of the BPNN mentioned in the previous section. Multiple optimization models have been developed and compared. The model with the smallest error has been determined as the damage recognition model of the bridge, and the training effect is shown in Fig. 14.

It can be observed from Fig.14 that when the number of hidden layer nodes is 12, the MSE is the smallest, the R2 is the highest and the training effect is the best. Thus, the model is selected as the damage identification model of the bridge based on GA-BPNN. In addition, the MSE of the optimized model is lower than that of the unoptimized model, and the R2 is higher than that of the unoptimized model, which means that the accuracy of the optimized model is better.

The steps of the optimization algorithm based on PSO include:

1) Build a BPNN model and randomly select the initial weights and thresholds.
2) Use particle swarm global search to find the best initial values of the BPNN.
3) Assign the optimal initial weights and thresholds to the BPNN to complete the optimization and make predictions.

The initial parameters of PSO are set as follows: the number of evolutionary generations is 50, the population size is 20, the crossover probability is 0.2, the velocity range is [-2,2], and the individual variation range is [-5,5]. The structure and relevant parameters of the BPNN used in the optimization algorithm are the same as those of the BPNN mentioned in the previous section. Multiple optimization models were built, compared, and the model with the smallest error was taken as the damage recognition model of Sanliushui bridge, and the training effect is shown in Fig. 14.

Similar to the training result of GA-BPNN, the training effect is best when n=12, and the accuracy of the optimized model is much better than the unoptimized model. Hence the model is selected as the damage identification of Sanliushui bridge based on PSO-BPNN.

The training effects of selected damage identification models based on BPNN, GA-BPNN, and PSO-BPNN are listed in Tab. 3. The data provided in Tab. 3 is applicable for all truck speeds and all acceleration measurement points mentioned

above. Despite the better training effect, the training time of PSO-BPNN is longer than that of GA-BPNN. Clearly, the MSE of the PSO-BPNN model is lower than that of the GA-BPNN model, while the R2 of the PSO-BPNN model is higher than that of the GA-BPNN model. However, the processing time of the PSO-BPNN model is longer than that of the GA-BPNN model.

Materials	BPNN	GA-BPNN	PSO-BPNN
MSE	0.00041639	0.00027874	0.00023449
R^2	0.93826	0.95867	0.96523
Training Time	4.420 s	12.667 s	54.571 s

Table 3: Training results of selected BPNN, GA-BPNN, and PSO-BPNN model.

In order to demonstrate the training results of BPNN, GA-BPNN, and PSO-BPNN models clearly, the original test data and the test data trained by the three models above are selected to draw the Taylor diagram, which is plotted in Fig. 15. Taylor diagram has the ability to compare the measured and predicted data and reflect the prediction ability of multiple models clearly by visualizing the standard deviation (SD) of multiple variables, the correlation coefficient (R2) with the reference value and the root-mean-square error (RMSE) comprehensively on a two-dimensional diagram [34].
Three statistical indices, SD, R2, and RMSE, are calculated as follows:

$$SD = \sqrt{\frac{\sum_{i=1}^{N}(X_i - \overline{X})^2}{N}} \tag{8}$$

$$RMSE = \sqrt{\frac{\sum_{i=1}^{N}(X_{mea} - X_{pre})^2}{N}} \tag{9}$$

$$R^2 = \left[\frac{\sum_{i=1}^{N}(X_{mea} - \overline{X}_{mea})(X_{pre} - \overline{X}_{pre})}{\sum_{i=1}^{N}(X_{mea} - \overline{X}_{mea})^2 \cdot \sum_{i=1}^{N}(X_{pre} - \overline{X}_{pre})^2}\right]^2 \tag{10}$$

where $Xmea$, $Xpre$, $\overline{X}mea$, and $\overline{X}pre$ are the measured, predicted, average measured, and average predicted values of the dataset, respectively.
As shown in Fig. 15, the test data trained by the BPNN, GA-BPNN, and PSO-BPNN models are similar to the original data in terms of radial distance from the dot, which means the simulation ability of the three models is similar, while the test data trained by the PSO-BPNN model is closest to the reference point representing the original data, indicating that the test data trained by the PSO-BPNN model is most correlated with the original data and has the smallest error.
The damage identification results by different truck speeds are close under the same location and machine learning method. For example, the damage identification results based on BPNN by different truck speeds in Tab. 4, the results are very close and then averaged to produce damage identification results applicable for various truck speeds. The damage identification results of Sanliushui bridges applicable for various truck speeds based on BPNN, GA-BPNN, PSO-BPNN, and load test data analysis method are most similar, and the errors do not exceed 10% as summarized by Tab. 5, which indicates that the proposed damage identification model is reliable.

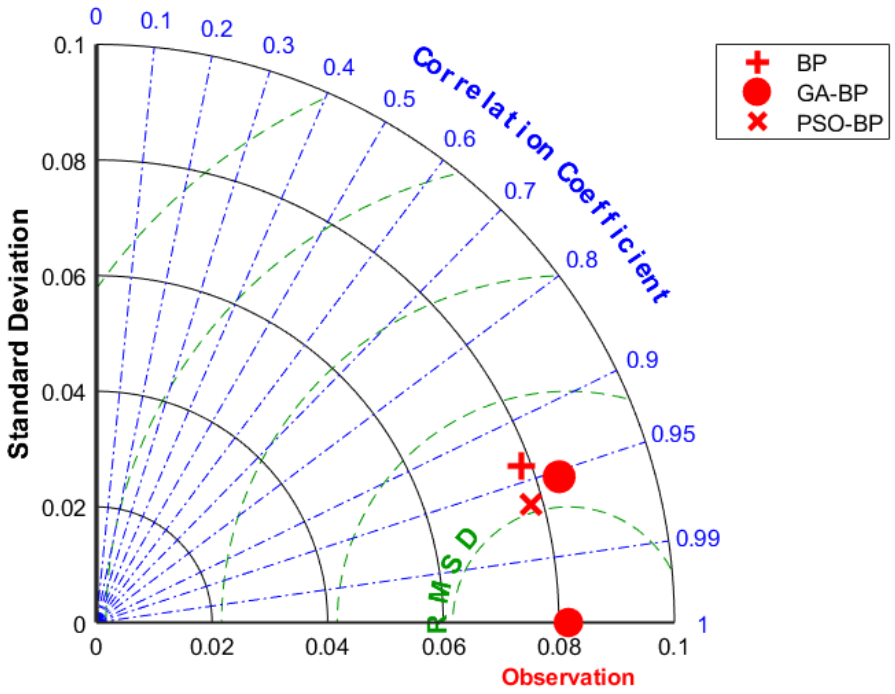

Fig.15: The Taylor diagram of original and trained data.

Materials	Point 1	Point 2	Point 3	Point 4	Point 5
30km/h	29.76%	32.13%	33.74%	25.21%	30.99%
40km/h	30.77%	34.27%	32.29%	28.53%	29.01%
50km/h	30.67%	30.06%	30.87%	22.66%	27.97%

Table 4: Training results of selected BPNN model for different truck speeds.

Materials	Point 1	Point 2	Point 3	Point 4	Point 5
BPNN	30.40%	32.15%	32.30%	25.47%	29.32%
GA-BPNN	31.45%	30.09%	31.79%	26.00%	28.58%
PSO-BPNN	31.57%	30.27%	32.20%	22.75%	28.18%
Test Data Analysis	30.00%	30.00%	30.00%	25.00%	30.00%

Table 5: Training results of selected BPNN, GA-BPNN, and PSO-BPNN model.

Conclusion

In this paper, an old arch bridge in Chenggu County was tested to identify its structural damage. The damage identification index has been developed according to wavelet packet analysis. WPERSS was applied to identify the damage. The test data and several ML methods were combined to obtain damage identification results. The conclusions are drawn as follows:

1) The damage degree of the second to the third spandrel arch are most severe (point 1-point 3), which are about 30%. The damage degree of the crown of the main arch (point 4) is about 25%.

2) The WPERSS value is positively correlated with the damage degree. Furtherly, the damage identification effect of the bridge damage identification method based on WPERSS value is not quite sensitive to the above factors: the number of measuring points, the damage degree of the measuring points, and the degree of wavelet packet decomposition or noise.

3) Training effects of optimized BPNN are significantly better than BPNN whose MSE is 0.00041639, R2 is 0.93826, and training time is 4.42015s when n=12. Among the optimization approaches, the training effect of PSO-BPNN is better than GA-BPNN in terms of consuming time, while the training time of PSO-BPNN is nearly 5 times as long as that of GA-BPNN. The MSE of PSO-BPNN is 0.00023449, which is 0.00004425 smaller than GA-BPNN. The R2 of PSO-BPNN is 0.96523, which is 0.00656 larger than GA-BPNN.

Acknowledgements

The authors are grateful for the support of Science and Technology Project of Department of Transport of Shaanxi Province (22-23K); Innovation and Entrepreneurship Training Program for College Students Research on Structural State and Degradation Mechanism of Stone Arch Bridges on Rural Roads (S20210712534).

References

[1] Figueiredo, E. and Brownjohn, J. (2022) Three decades of statistical pattern recognition paradigm for SHM of bridges. Structural Health Monitoring 21(6), pp. 3018-3054. DOI: 10.1177/14759217221075241.

[2] Rizzo, P. and Enshaeian, A. (2021) Challenges in bridge health monitoring: A review. Sensors 21(13):4336. DOI: 10.3390/s21134336.

[3] Goyal, D. and Pabla, B. S. (2016) The vibration monitoring methods and signal processing techniques for structural health monitoring: a review. Archives of Computational Methods in Engineering, 23(4), pp. 585-594. DOI: 10.1007/s11831-015-9145-0.

[4] Facchini, G., Bernardini, L., Atek, S. and Gaudenzi, P. (2015) Use of the wavelet packet transform for pattern recognition in a structural health monitoring application. Journal of Intelligent Material Systems and Structures 26(12), pp. 1513-1529. DOI: 10.1177/1045389X14544146.

[5] Kankanamge, Y., Hu, Y. and Shao, X. (2020) Application of wavelet transform in structural health monitoring. Earthquake Engineering and Engineering Vibration, 19(2), 515-532. DOI: 10.1007/s11803-020-0576-8.

[6] Zhu Jinsong, Sun Yadan (2015) Wavelet Packet Energy Based Damage Detection Index for Bridge (In Chinese). Journal of Vibration, Measurement & Diagnosis 5(04), pp. 715-721+800. DOI: 10.16450/j.cnki.issn.1004-6801.2015.04.019.

[7] Yue Pan, Limao Zhang, Xianguo Wu, Kainan Zhang, Miroslaw J. Skibniewski (2019) Structural health monitoring and assessment using wavelet packet energy spectrum. Safety Science 120, pp. 652-665. DOI: 10.1016/j.ssci.2019.08.015.

[8] Sun L, Shang Z, Xia Y, et al. (2020) Review of bridge structural health monitoring aided by big data and artificial intelligence: From condition assessment to damage detection. Journal of Structural Engineering 2020 (5), 04020073. DOI: 10.1061/(ASCE)ST.1943-541X.0002535.

[9] Malekloo A, Ozer E, AlHamaydeh M, et al. (2022) Machine learning and structural health monitoring overview with emerging technology and high-dimensional data source highlights. Structural Health Monitoring 21(4), pp. 1906-1955. DOI: 10.1177/14759217211036880.

[10] Moisés Silva, Adam Santos, Eloi Figueiredo, et al. (2016) A novel unsupervised approach based on a genetic algorithm for structural damage detection in bridges. Engineering Applications of Artificial Intelligence 52, pp. 168-180. DOI: 10.1016/j.engappai.2016.03.002.

[11] Osama Abdeljaber, Onur Avci, Mustafa Serkan Kiranyaz, et al. (2018) 1-D CNNs for structural damage detection: Verification on a structural health monitoring benchmark data. Neurocomputing 275, pp. 1308-1317. DOI: 10.1016/j.neucom.2017.09.069.

[12] Liu, J., Li, P., Tang, X. et al. (2021) Research on improved convolutional wavelet neural network. Sci Rep 11, 17941. DOI: 10.1038/s41598-021-97195-6.

[13] Tran-Ngoc H, Khatir S, Ho-Khac H, et al. (2021) Efficient Artificial neural networks based on a hybrid metaheuristic optimization algorithm for damage detection in laminated composite structures. Composite Structures 262, 113339. DOI: 10.1016/j.compstruct.2020.113339.
[14] Flah, M., Nunez, I., Ben Chaabene, W. and Nehdi, M. L. (2021). Machine learning algorithms in civil structural health monitoring: a systematic review. Archives of computational methods in engineering, 28, pp. 2621-2643. DOI: 10.1007/s11831-020-09471-9.
[15] Gui G, Pan H, Lin Z, et al. (2017) Data-driven support vector machine with optimization techniques for structural health monitoring and damage detection. KSCE Journal of Civil Engineering 21(2), pp. 523-534. DOI: 10.1007/s12205-017-1518-5.
[16] Santarsiero G, Mishra M, Singh M K, et al. (2021) Structural health monitoring of exterior beam–column subassemblies through detailed numerical modelling and using various machine learning techniques. Machine Learning with Applications 6, 100190. DOI: 10.1016/j.mlwa.2021.100190.
[17] Zhou, K., Lei, D., He, J., et al. (2021). Real-time localization of micro-damage in concrete beams using DIC technology and wavelet packet analysis. Cement and Concrete Composites, 123, 104198. DOI: 10.1016/j.cemconcomp.2021.104198.
[18] Ministry of Transport of the People's Republic of China (2015) General Specifications for Design of Highway Bridges and Culverts: JTG D60-2015. (In Chinese)
[19] Xia, Z., Lin, Y., Wang, Q., et al. (2021). Damage detection method for cables based on the change rate of wavelet packet total energy and a neural network. Journal of Civil Structural Health Monitoring, 11, pp. 593-608. DOI: 10.1007/s13349-021-00471-2.
[20] Ministry of Environmental Protection of the People's Republic of China (2008) Environmental Quality Standard for Noise: GB 3096-2008. (In Chinese)
[21] Xiong, Z., Li, J., Zhu, H., Liu, X. and Liang, Z. (2022) Ultimate bending strength evaluation of mvft composite girder by using finite element method and machine learning regressors. Latin American Journal of Solids and Structures, 19(3), pp. 1-20. DOI: 10.1590/1679-78257006.
[22] Kashem M A, Akhter M N, Ahmed S, et al. (2011) Face recognition system based on principal component analysis (PCA) with back propagation neural networks (BPNN). Canadian Journal on Image Processing and Computer Vision 2(4), pp. 36-45.
[23] Li, S., Wang, W., Lu, B., Du, et al. (2022) Long-term structural health monitoring for bridge based on back propagation neural network and long and short-term memory. Structural Health Monitoring, 14759217221122337. DOI: 10.1177/14759217221122337.
[24] Shu, J., Zhang, Z., Gonzalez, I. and Karoumi, R. (2013) The application of a damage detection method using Artificial Neural Network and train-induced vibrations on a simplified railway bridge model. Engineering structures 52, pp. 408-421. DOI: 10.1016/j.engstruct.2013.02.031.
[25] Flah, M., Nunez, I., Ben Chaabene, W. and Nehdi, M. L. (2021) Machine learning algorithms in civil structural health monitoring: a systematic review. Archives of computational methods in engineering, 28(4), pp. 2621-2643. DOI: 10.1007/s11831-020-09471-9.
[26] Xiong Z, Zhu H, Li W, et al. (2022) Seismic Risk Assessment of a Novel Bridge-Aqueduct Cobuilt Structure. ASCE-ASME Journal of Risk and Uncertainty in Engineering Systems, Part A: Civil Engineering 8(3), 04022022. DOI: 10.1061/AJRUA6.0001245.
[27] Yile Ao, Hongqi Li, Liping Zhu, Sikandar Ali and Zhongguo Yang. (2019) The linear random forest algorithm and its advantages in machine learning assisted logging regression modeling. Journal of Petroleum Science and Engineering 174, pp. 776-789. DOI: 10.1016/j.petrol.2018.11.067.
[28] Zhang, Y., Xiong, Z., Liang, Z., She, J., Ma, C. (2023). Structural Damage Identification System Suitable for Old Arch Bridge in Rural Regions: Random Forest Approach. CMES-Computer Modeling in Engineering & Sciences, 136(1), pp. 447–469. DOI: 10.32604/cmes.2023.022699.
[29] Sahoo, S.K., Saha, A.K. (2022) A Hybrid Moth Flame Optimization Algorithm for Global Optimization. Journal of Bionic Engineering 19, pp. 1522–1543. DOI: 10.1007/s42235-022-00207-y.
[30] Yan, Z., Zhang, J., Zeng, J. and Tang, J. (2021) Nature-inspired approach: An enhanced whale optimization algorithm for global optimization. Mathematics and Computers in Simulation 185, pp. 17-46. DOI: 10.1016/j.matcom.2020.12.008.
[31] Mirjalili, S. (2019) Genetic algorithm//Evolutionary algorithms and neural networks. Springer, Cham, pp. 43-55. DOI: 10.1016/j.matcom.2020.12.008.

[32] Wang, D., Tan, D., Liu, L. (2018) Particle swarm optimization algorithm: an overview. Soft computing 22(2), pp. 387-408. DOI: 10.1007/s00500-016-2474-6.

[33] Zhang, P., and Chuanhe, S. (2019) Choice of the number of hidden layers for back propagation neural network driven by stock price data and application to price prediction. Journal of Physics: Conference Series 1302(2). DOI: 10.1088/1742-6596/1302/2/022017.

[34] Yafouz, A., Ahmed, A. N., Zaini, N. A., et al. (2021). Hybrid deep learning model for ozone concentration prediction: Comprehensive evaluation and comparison with various machine and deep learning algorithms. Engineering Applications of Computational Fluid Mechanics, 15(1), pp. 902-933. DOI: 10.1080/19942060.2021.1926328.